ACS OMEGA

http://pubs.acs.org/journal/acsodf

Article

Organic Geochemical Characteristics and Organic Matter Enrichment of the Upper Permian Longtan Formation Black Shale in Southern Anhui Province, South China

Jianghui Ding,* Jinsheng Sun, Haikuan Nie,* Xiangtong Yang, Yu Ye, Gang Shi, Ruyi Wang, Bo Huang, Xun Sun, and Huili Li

Cite This: *ACS Omega* 2023, 8, 16748−16761

Read Online

ACCESS | Metrics & More | Article Recommendations

ABSTRACT: Although previous studies have yielded valuable insights into shale gas reservoirs, a comprehensive understanding of the organic geochemical characteristics and organic matter enrichment of marine−continental transitional shale has yet to be achieved. The Longtan Formation transitional shales were extensively deposited in Southern Anhui Province, South China, during the Late Permian. Our analysis of twenty-two rock samples from one core (Gangdi-1 well) and two outcrops (Daoshanchong outcrop and Changqiao outcrop) revealed that the Longtan Formation shale extracts exhibit a wide range of C_{11}−C_{35} *n*-alkanes and acyclic isoprenoids, with unimodal, bimodal, and multimodal distributions. The carbon peak ranges from nC_{15} to nC_{24}, with high quantities of medium-chain *n*-alkanes (nC_{22}−nC_{25}), indicating that the organic matter in Longtan Formation shale originates from a mixed source of higher plant debris and lower aquatic organisms. Our conclusion is supported by the ternary diagram of C_{27}−C_{28}−C_{29} regular steranes and the variations of the $\delta^{13}C$ values of C_{15}−C_{32} *n*-alkanes, which is higher than the corresponding value (<1.6‰) of *n*-alkanes from a single source. Furthermore, thermal maturity proxies based on organic petrography (R_o and T_{max}) and biomarkers, such as the ratios of C_{31} 22S/(22S + 22R), C_{29} 20S/(20S + 20R), and C_{29} $\beta\beta/(\alpha\alpha + \beta\beta)$, suggest that organic matter is in a mature stage of hydrocarbon generation. By analyzing the Pr/Ph ratio and pyrite morphology combined with a plot of total organic carbon (TOC) versus total sulfur (TS) and the Pr/nC_{17}−Ph/nC_{18} diagram, we speculate that the Longtan Formation shales were chiefly developed in a dysoxic-to-oxic water environment. Finally, we establish depositional models of organic matter enrichment in deltaic and tidal flat-lagoon environments, emphasizing that the abundant mixed-sourced organic matter can significantly enhance primary productivity, and a higher sedimentation rate can distinctly shorten organic matter exposure time in the oxidized water environment, thereby promoting organic matter accumulation in such a setting.

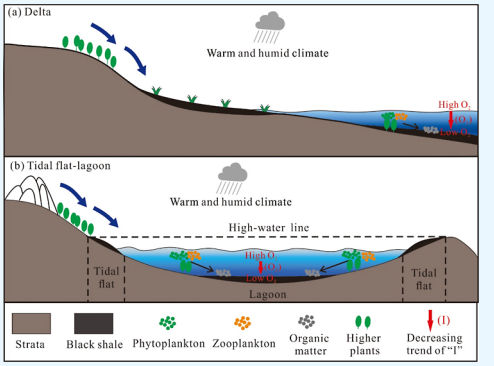

1. INTRODUCTION

Black shales are widespread in South China, particularly in the Yangtze plate.[1−5] These black rock strata incorporate various metallic deposits and are also the targets for shale oil and gas exploration and development.[6−8] The Southern Anhui Province, located in the core area of the Yangtze River Economic Belt, has experienced a rapid economic development but suffers from a serious energy resource deficiency. The transitional shale in the upper Permian Longtan Formation is a crucial hydrocarbon source rock in South China and exhibits favorable geological conditions for shale gas accumulation.[4,5,7,9−12] Recent exploration in the region has included the drilling of several survey wells, such as Gangdi-1 well and Jingye-1 well, revealing shale gas discoveries in the upper Permian strata and attracting significant attention in China.[7,13] Despite possessing substantial shale gas potential, shale gas exploration in Southern Anhui Province has yet to achieve a significant breakthrough.[11,14] Previous research works have demonstrated that Longtan Formation transitional shales have considerable thickness, a high total organic carbon (TOC) content, medium maturity, well-developed nanopores, high clay mineral contents, and relatively high gas contents, making them excellent hydrocarbon source rocks and primary exploration targets for shale gas in Southern Anhui Province, South China.[6,9,11,14] However, the systematic understanding of organic matter enrichment during the transitional shale deposition in this setting is still lacking and needs to be clarified in order to provide a valid geological foundation for shale gas exploration in Southern Anhui Province in future.[7,9,12,15]

Received: January 14, 2023
Accepted: April 20, 2023
Published: May 2, 2023

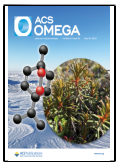

Over the past few decades, extensive research works have been conducted on the geochemical characteristics and organic matter enrichment in marine sediments.[16−18] It is widely accepted that special geological conditions are required for organic matter accumulation in marine sediments, and no single process or model can explain organic matter accumulation in all sedimentary environments due to the complex geological history. Moreover, environmental fluctuations are more common in transitional settings than in marine systems, likely due to the relatively small sizes of water reservoirs.[11,19,20] The Longtan Formation transitional shales, which were deposited in delta and tidal flat-lagoon environments, exhibit strong vertical and horizontal heterogeneities in geochemical characteristics,[5,7,12,21] making them an invaluable opportunity to study organic geochemical characteristics and explore organic matter enrichment in such environments.[12,15] Specifically, the biomarker distribution can provide molecular-level information on organic matter sources, thermal maturity, and organic matter enrichment.[23−28]

In the present study, we conducted a comprehensive analysis of the organic geochemistry, mineral composition, and pyrite morphology on Longtan Formation rock samples collected from one core (Gangdi-1 well) and two outcrops (Daoshanchong outcrop and Changqiao outcrop) in South China. Our primary objectives are as follows: (1) to provide a detailed organic geochemical characterization; (2) to analyze the organic matter sources, thermal maturity, and palaeoredox conditions; and (3) to establish depositional models of organic matter accumulation in deltaic and tidal flat-lagoon environments. These findings would offer valuable insights into shale gas exploration in South China.

2. GEOLOGIC SETTING

The Southern Anhui Province is situated in the Lower Yangtze area (Figure 1) and is a promising region for shale oil and gas exploration and exploitation in South China.[6,7,13] The strata have been deposited with a thickness of over 10,000 m in Southern Anhui Province since the Paleozoic. A simplified stratigraphic histogram of the Lower Yangtze platform is shown in Figure 2a. Previous studies suggest that the studied area was mainly developed in a transitional environment during the Late Permian Wuchiapingian.[6,7] The strata in Longtan Formation (P_3l) are primarily formed in such a setting.[6] A series of black rocks were deposited in Longtan Formation, mainly including shale, mudstone, siltstone, fine sandstone, and limestone intercalated with thin coal seams. The Longtan Formation transitional shales are extensively distributed in Southern Anhui Province and are considered high-quality hydrocarbon source rocks in South China.[4,5,9] Based on the lithostratigraphic unit, Longtan Formation can be further divided into three components: lower, middle, and upper Longtan intervals. The lower and upper intervals were mainly formed in a delta sedimentary system, while the middle interval was chiefly deposited in a tidal flat-lagoon system.[7]

The Gangdi-1 well, located in the Jing County of Xuancheng City in Anhui Province (Figure 1), has a total depth of over 1500 m and consists of Gufeng Formation (P_2g), Longtan Formation (P_3l), Dalong Formation (P_3d), and Yinkeng Formation (T_1y) in descending order. The Longtan Formation of Gangdi-1 well is located at a depth of 986.7−1195.0 m and comprises approximately 40.0 m of black shale. Specifically, this study focuses on the lower Longtan Formation of Gangdi-1 well (Figure 2b), which is dominated by black mudstone and shale,

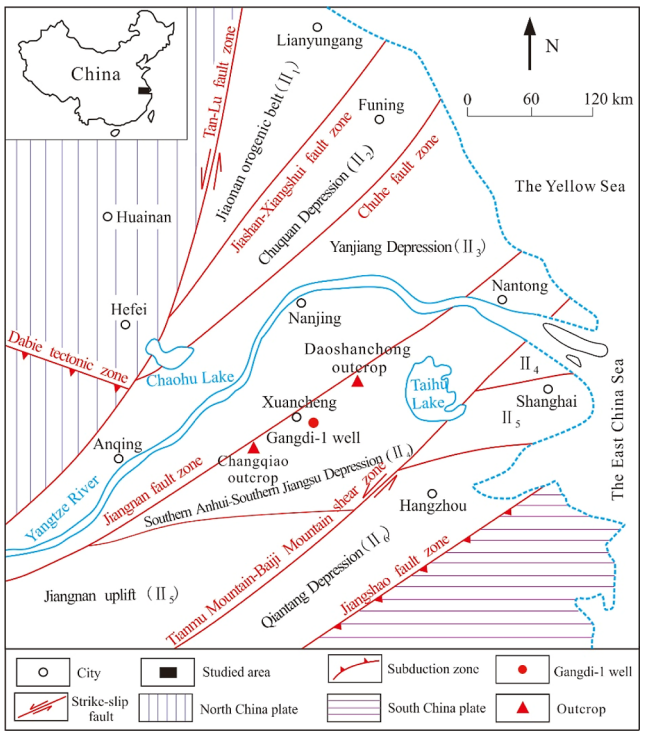

Figure 1. Location map of the sampling well and outcrops in the Lower Yangtze area.

gray-black siltstone (Figure 3a), and gray fine sandstone interbedded with thin coal seams in a delta sedimentary system at a depth of 1109.1−1195.0 m. A number of micro-fractures with a width of 0.01−0.05 mm can be observed in thin sections (Figure 3g).

The Daoshanchong outcrop and the Changqiao outcrop are also situated in the Jing County of Xuancheng City in Southern Anhui Province (Figure 1). The uncovered strata in the Daoshanchong outcrop with a total thickness of 14.8 m are formed in the middle Wuchiapingian stage (Figure 2b) and dominated by carbonaceous shale (Figure 3b,c) and limestone, which are considered to be deposited in tidal flat-lagoon facies. Analogously, the uncovered strata in the Changqiao outcrop with a total thickness of 25.0 m are deposited in the late Wuchiapingian stage (Figure 2b) and are chiefly composed of mudstone, shale, and siltstone (Figure 3d−f), which are thought to be developed in a delta sedimentary system. A large number of micro-fractures with a width of 0.01−2.0 mm can be observed in thin sections, most of which are filled by calcite and quartz (Figure 3h,i).

3. SAMPLES AND METHODS

3.1. Samples. Twenty-two rock samples were collected from the Gangdi-1 well (GD-1 to GD-6), Daoshanchong outcrop (DSC-1 to DSC-6), and Changqiao outcrop (CQ-1 to CQ-10) for analysis of organic geochemistry, mineral composition, and pyrite morphology. All these samples were subject to TOC analysis. Taking into account the TOC variation, sample quantity, and its distribution throughout the Longtan interval, the selected samples were analyzed for total sulfur (TS), vitrinite reflectance (R_o), Rock-Eval pyrolysis, gas chromatography (GC), gas chromatography−mass spectrometry (GC−MS), $\delta^{13}C$ values of individual *n*-alkanes, mineral composition, and pyrite morphology.

https://doi.org/10.1021/acsomega.3c00273
ACS Omega 2023, 8, 16748−16761

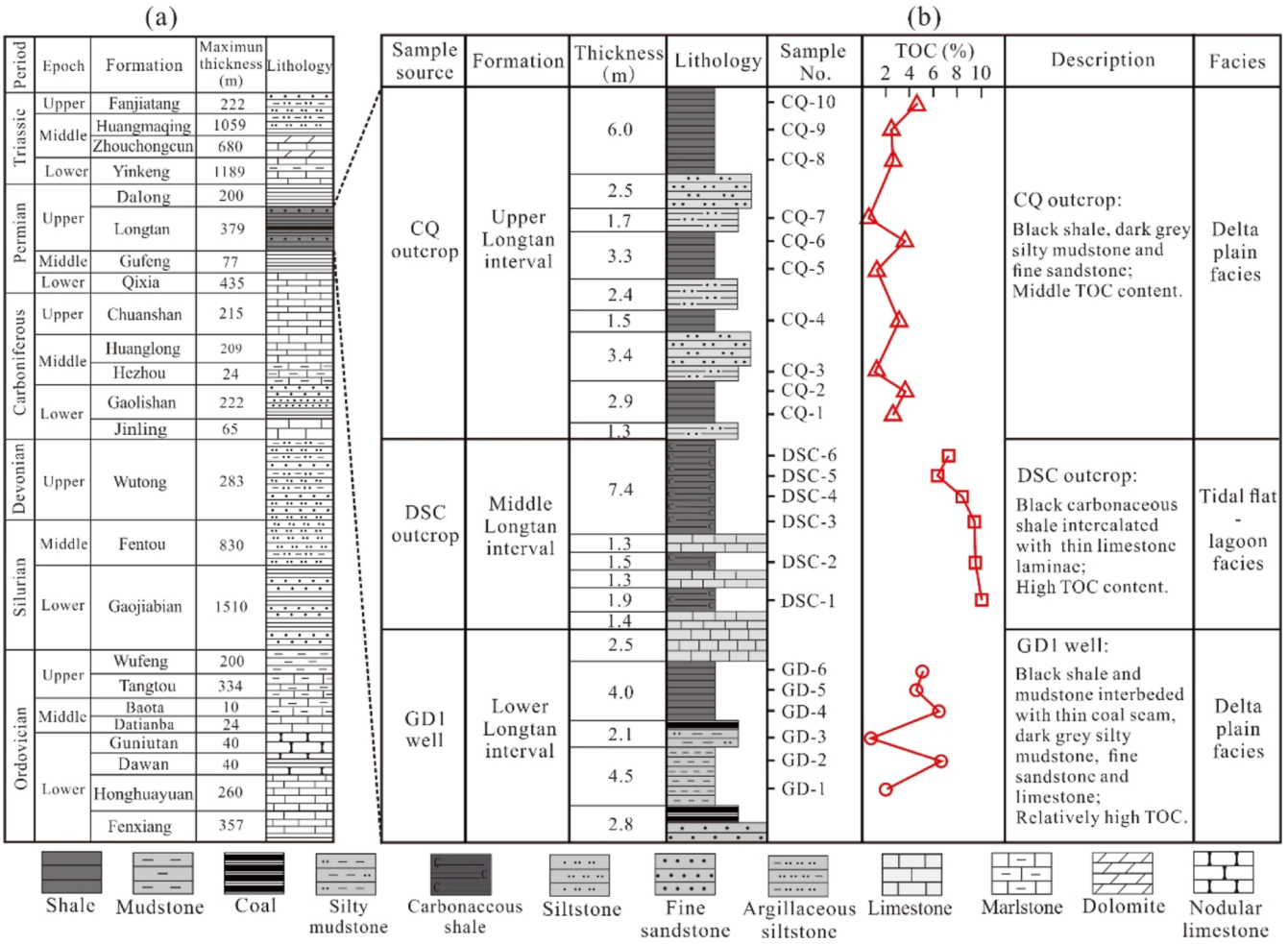

Figure 2. Stratigraphic histogram of (a) Paleozoic and (b) the upper Permian Longtan Formation based on the Gangdi-1 (GD1) well, Daoshanchong (DSC) outcrop, and Changqiao (CQ) outcrop in Southern Anhui Province.

3.2. Methods. *3.2.1. Organic Matter Geochemistry.* TOC and TS were analyzed using a LECO CS-400 instrument, following the method described by Ding et al.[29] and Mansour et al.,[28] respectively. Vitrinite reflectance (R_o) was determined on whole-rock powdered samples using a Leitz MPV-SP microphotometer with an oil-immersion objective lens, according to the method described by Schoenherr et al.[30] Rock-Eval pyrolysis was conducted on a Rock-Eval VI instrument in accordance with the procedure outlined by Carvajal-Ortiz and Gentzis.[31] GC–MS analysis of the saturated hydrocarbon fraction was performed using an Agilent 7890A gas chromatograph coupled to an HP-5 column, following the method and procedure described by Ding et al.[18] The $\delta^{13}C$ values of individual *n*-alkanes were obtained using an Agilent 7890A gas chromatograph equipped with a Finnigan Delta V isotope ratio mass spectrometer, according to the procedure depicted by Ding et al.[18]

3.2.2. XRD Analysis. Powdered samples with a grain size of less than 75 μm (200 mesh) were utilized for X-ray diffraction (XRD) analysis, which was performed on a Bruker D8 Discover with an operating voltage at 40 kV and a working current at 30 mA. Each XRD pattern was obtained using Ni-filtered Cu Kα radiation in a step mode with a step size of 0.02°. Mineral identification and weight percentages of different minerals were obtained through computer analysis of the diffractograms.

3.2.3. SEM Observation. A total of eight rock samples were utilized to investigate the pyrite characteristics. Initially, these samples were mechanically polished to prepare thin sections and to examine the pyrite morphology and measure the framboid diameter using an FEI Quanta 200 field emission scanning electron microscope. Subsequently, the thin sections were further polished with an argon ion mill to create a flat artifact-free surface that is better suitable for gaining high-resolution images. Finally, the polished samples were observed in a high-pressure vacuum chamber, where the pyrite framboids could be readily identified by their morphology.

4. RESULTS

4.1. Bulk Geochemical Characteristics. With TOC values ranging from 0.96% to 9.54% for the ten target samples (Table 1), most of the samples can be classified as "Very Good Source Rock (2.0% < TOC < 4.0%)" to "Excellent Source Rock (TOC > 4.0%)" based on their organic matter richness.[32,33] Notably, TOC contents vary among different sedimentary systems. Specifically, the target samples collected from the Daoshanchong section, which were deposited in a tidal flat-lagoon system, exhibited high TOC contents ranging from 7.32% to 9.54% (average 8.42%; Table 1). In contrast, the rock samples from the Gangdi-1 well and Changqiao section, both of which developed in a delta sedimentary system, showed medium TOC contents ranging from 0.96% to 6.70% (average 3.69%; Table 1),

https://doi.org/10.1021/acsomega.3c00273
ACS Omega 2023, 8, 16748−16761

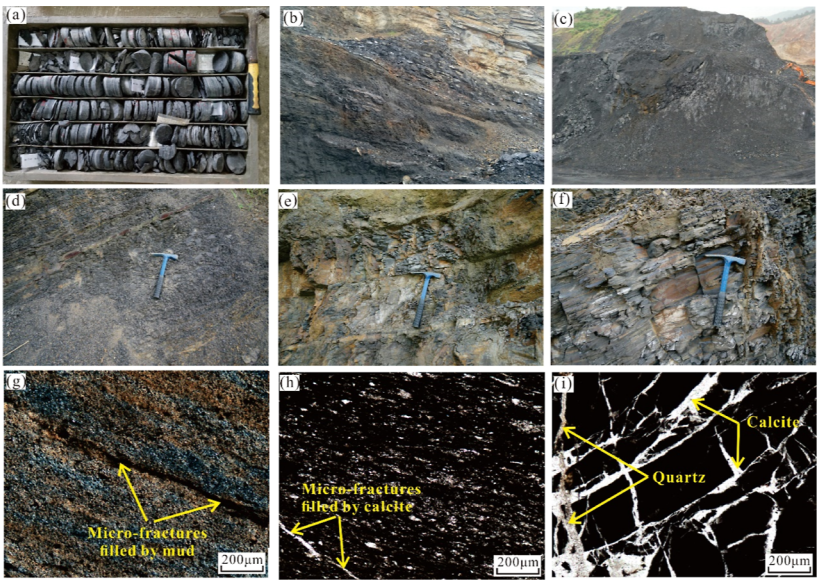

Figure 3. Photographs and thin sections of Longtan Formation siliceous rocks in Southern Anhui Province. (a) Thick gray-black siltstone interbedded with thin sandstone lamina, 1188.1−1192.6 m, Gangdi-1 well; (b,c) panoramic view of the Daoshanchong outcrop; (d) gray-black silty mudstone interbedded with thin sandstone lamina, Changqiao outcrop; (e) thick gray black shale intercalated with thin siltstone, Changqiao outcrop; (f) black-gray silty mudstone, Changqiao outcrop; (g) micro-fractures with a width of 0.01−0.05 mm filled by mud under cross-polarized light, GD-1; (h) micro-fractures with a width of 0.01−0.05 mm filled by calcite under plane-polarized light, CQ-4; (i) micro-fractures with a width of 0.01−2.0 mm filled by calcite and quartz under plane-polarized light, CQ-6.

Table 1. TOC, TS, R_o, and Rock-Eval Pyrolysis Data of Longtan Formation Rock Samples in Southern Anhui Province[a]

sample ID	TOC	TS	R_o	S_1	S_2	S_3	T_{max}	HI	OI	PI
CQ-8	2.63	0.92	1.42	0.13	0.30	0.11	459	11.41	4.18	0.30
CQ-6	3.74	1.07	1.38	1.17	2.98	0.36	442	79.68	9.63	0.28
CQ-4	3.29	0.89	1.34	0.27	0.61	0.53	449	18.54	16.11	0.31
DSC-6	7.32	1.54	1.49	0.12	0.17	0.91	469	2.32	12.43	0.41
DSC-4	8.39	1.72	1.57	0.09	0.16	1.68	485	1.91	20.02	0.36
DSC-2	9.54	1.91	1.63	0.07	0.15	0.84	496	1.57	8.81	0.32
GD-4	6.45	1.73	1.23	0.24	0.13	0.22	435	2.02	3.41	0.65
GD-3	0.96	0.81	1.24	0.06	0.11	0.17	441	11.46	17.71	0.35
GD-2	6.70	1.26	1.47	0.12	0.14	0.20	485	2.09	2.99	0.46
GD-1	2.03	0.74	1.31	0.21	0.07	0.37	453	3.45	18.23	0.75
average	5.11	1.26	1.41	0.25	0.48	0.54	461	13.44	11.35	0.42

[a]Note: TOC: total organic carbon, %; TS: total sulfur, %; R_o: vitrinite reflectance, %; S_1: free hydrocarbon content, mg HC/g rock; S_2: remaining hydrocarbon generative potential, mg HC/g rock; S_3: CO_2 content during pyrolysis, mg CO_2/g rock; T_{max}: temperature of maximum hydrocarbon generation, °C; HI (hydrogen index) = 100 × S_2/TOC, mg HC/g TOC; OI (oxygen index) = 100 × S_3/TOC, mg CO_2/g TOC; PI (production index) = $S_1/(S_1 + S_2)$.

Table 2. Parameters of *n*-Alkanes (m/z 85) for Longtan Formation Rock Samples in Southern Anhui Province[a]

sample ID	carbon peak	nC_{21}^-/nC_{22}^+	OEP	Pr/Ph	Pr/nC_{17}	Ph/nC_{18}	TAR
CQ-8	nC_{22}	0.54	0.92	1.02	0.84	0.15	1.38
CQ-6	nC_{20}	0.39	1.02	1.85	0.74	0.05	2.46
CQ-4	nC_{24}	0.51	1.08	1.25	0.66	0.21	1.53
DSC-6	nC_{24}	0.46	0.87	1.53	0.71	0.27	1.65
DSC-4	nC_{20}	0.83	1.06	0.96	0.85	0.13	0.41
DSC-2	nC_{19}	0.56	0.94	1.06	0.63	0.21	1.19
GD-4	nC_{19}	0.85	1.07	1.07	0.51	0.33	0.72
GD-3	nC_{17}	1.41	0.99	1.83	0.44	0.25	0.33
GD-2	nC_{15}	2.15	1.04	1.80	0.61	0.38	0.23
GD-1	nC_{18}	1.34	0.98	1.18	0.51	0.39	0.31
average		0.90	1.00	1.36	0.65	0.24	1.02

[a]Note: TAR (terrigenous/aquatic ratio): $(nC_{27} + nC_{29} + nC_{31})/(nC_{15} + nC_{17} + nC_{19})$.

https://doi.org/10.1021/acsomega.3c00273
ACS Omega 2023, 8, 16748−16761

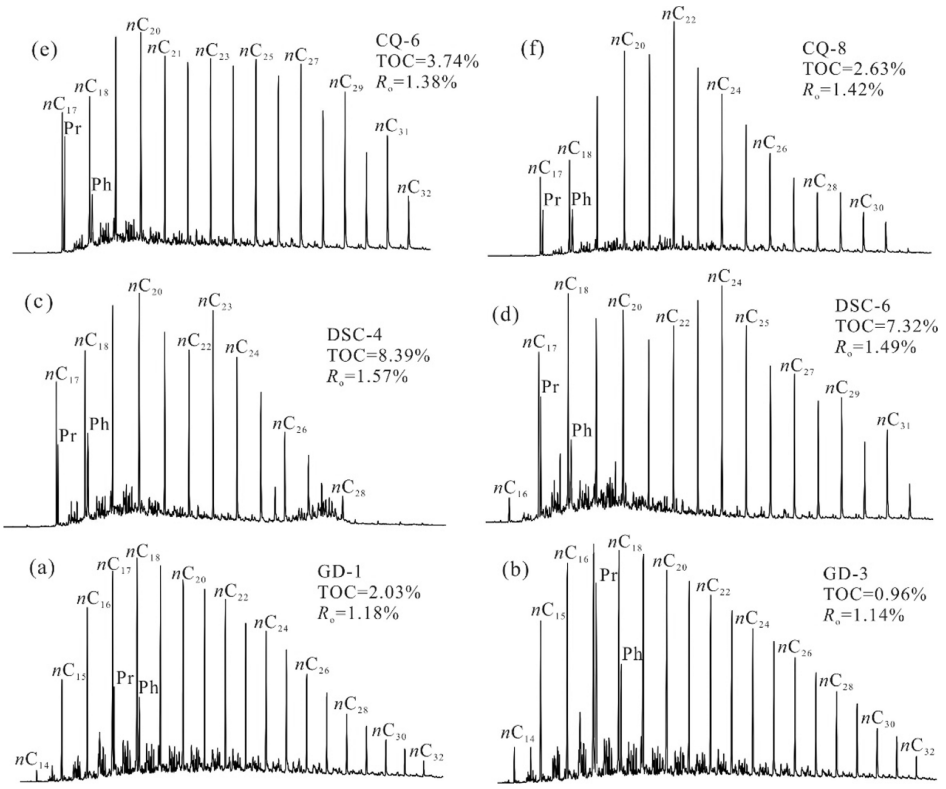

Figure 4. Mass chromatograms (a–f) of saturated hydrocarbons at m/z 85 for Longtan Formation rock samples from the Gangdi-1 well and two outcrops in Southern Anhui Province.

being significantly lower than those of the Daoshanchong outcrop. Additionally, TS exhibited relatively lower values ranging from 0.74% up to 1.91% (average 1.26%) throughout the Longtan interval, probably suggesting that only a small quantity of pyrites was produced during the process of shale deposition.[28,34,35]

The Longtan Formation shale samples exhibit a mature stage of hydrocarbon generation as indicated by their vitrinite reflectance (R_o) in the range of 1.23%–1.63% (average 1.41%) and T_{max} values ranging from 435 to 496 °C (average 461 °C).[36] The R_o and T_{max} values of Longtan Formation shales collected from the Gangdi-1 well, Daoshanchong outcrop, and Changqiao outcrop exhibit no significant differences (Table 1), suggesting the consistent thermal maturation of organic matter in these shales. Moreover, the HI (hydrogen index), OI (oxygen index), and PI (production index) values are in the range of 1.57–79.68 mg HC/g TOC (average, 13.44 mg HC/g TOC), 2.99–20.02 mg CO_2/g TOC (average, 11.35 mg CO_2/g TOC), and 0.28–0.75 (average, 0.42) (Table 1), respectively.

4.2. Biomarker Distribution. *4.2.1. Normal Alkanes (n-Alkanes) and Isoprenoids.* The mass chromatograms of saturated hydrocarbons at m/z 85 for ten samples exhibit a broad range of C_{11}–C_{35} n-alkanes and acyclic isoprenoids, with distinct differences observed among samples from different sources (layers). Specifically, the rock samples collected from the Gangdi-1 well display a unimodal distribution of n-alkanes with the carbon peak within the range of nC_{15}–nC_{19} (Table 2 and Figure 4a–f), while samples from the Daoshanchong outcrop and Changqiao outcrop show bimodal or multimodal distributions of n-alkanes with the carbon peak ranging from nC_{19} to nC_{24} (Table 2 and Figure 4c–f). The nC_{21}^-/nC_{22}^+ ratio is utilized to recognize variations in the relative abundance of light and heavy hydrocarbons.[37,38] Results indicate that Longtan Formation shale samples have relatively low nC_{21}^-/nC_{22}^+ ratios varying from 0.39 to 2.15, with an average of 0.90 (Table 2). Odd-over-even predominance (OEP) is used to determine the organic matter source and thermal maturity.[32,39] The OEP values range from 0.87 to 1.08, with an average of 1.00 (Table 2), suggesting that Longtan Formation shales do not exhibit any obvious odd and even carbon number predominance. Pr and Ph are important and practical acyclic isoprenoid compounds.[32,38,40,41] The relatively low Pr/Ph ratios of the target samples are likely associated with the thermal evolution process and different sources of Pr and Ph.[38] Additionally, the relatively lower abundances of acyclic isoprenoids compared to n-alkanes are reflected in the Pr/nC_{17} and Ph/nC_{18} ratios ranging from 0.44 to 0.85 (average, 0.65; Table 2) and 0.05 to 0.39 (average, 0.24; Table 2), respectively.

4.2.2. Terpanes. The mass chromatograms of saturated hydrocarbons at m/z 191 for the target samples revealed the presence of various terpanes, including tricyclic terpanes ranging from C_{19} to C_{29} (with C_{23} being the dominant component), C_{30}-hopane, C_{29}-norhopane, Ts, Tm, gammacerane, as well as homohopanes (C_{31}–C_{35}) and tetracyclic terpanes in low quantities (Figure 5a–d). It is worth noting that the concentration of C_{30}-hopane is higher than that of C_{29}-norhopane, with low C_{29}-norhopane/C_{30}-hopane ratios ranging from 0.44 to 0.56 (average, 0.50; Table 3). The relative abundances of Tm and Ts are almost equal, with Tm/Ts ratios in the range of 0.63–1.29 (average, 1.03; Table 3). Furthermore, Ts/(Ts + Tm) ratios range from 0.44 to 0.61, suggesting a late hydrocarbon generation stage.[26,42] Additionally, gammacerane is present in all the target samples with a medium abundance (Figure 5a–d). The gammacerane index (GI), calculated as GI = gammacerane/C_{30}-hopane, is an indicator of water column stratification and is likely related to salinity or temper-

https://doi.org/10.1021/acsomega.3c00273
ACS Omega 2023, 8, 16748–16761

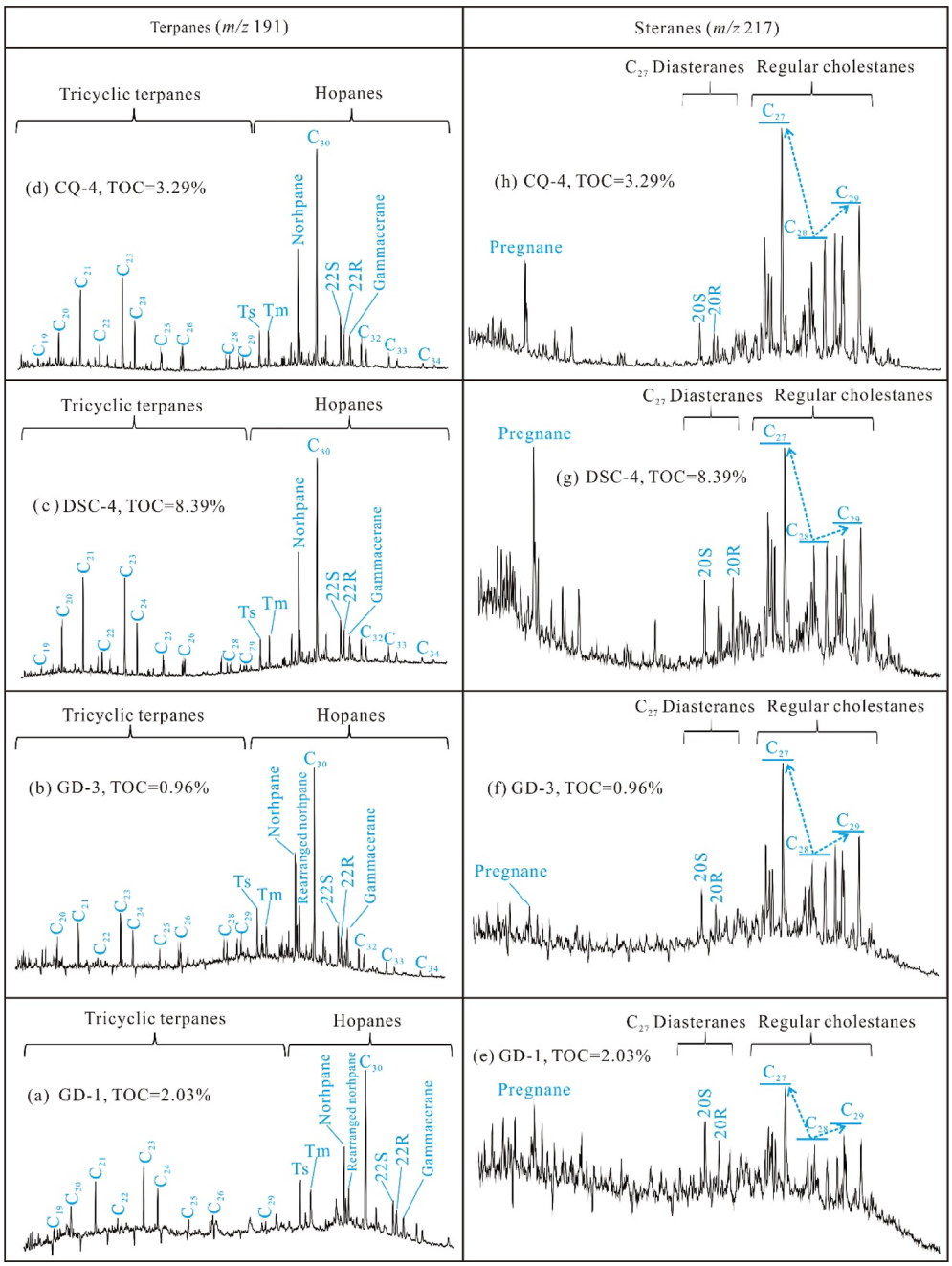

Figure 5. Mass chromatograms of terpanes (a−d) and steranes (e−h) for Longtan Formation shale samples in Southern Anhui Province.

Table 3. Parameters of Terpanes (*m*/*z* 191) for Longtan Formation Rock Samples in Southern Anhui Province[a]

sample ID	$C_{29}/C_{30}H$	Tm/Ts	Ts/(Ts + Tm)	GI	$C_{24}Te/C_{23}T$	C_{31} 22S/(22S + 22R)
CQ-8	0.46	1.19	0.46	0.21	0.29	0.59
CQ-6	0.49	1.03	0.49	0.16	0.20	0.59
CQ-4	0.50	1.15	0.47	0.19	0.20	0.58
DSC-6	0.48	1.12	0.47	0.18	0.18	0.52
DSC-4	0.46	1.02	0.49	0.17	0.19	0.58
DSC-2	0.52	1.22	0.45	0.21	0.17	0.57
GD-4	0.51	0.79	0.57	0.24	0.31	0.60
GD-3	0.53	0.63	0.61	0.25	0.35	0.58
GD-2	0.56	0.88	0.53	0.27	0.07	0.41
GD-1	0.44	1.29	0.44	0.18	0.42	0.55
average	0.50	1.03	0.50	0.21	0.24	0.56

[a]Note: C_{29}: C_{29}-norhopane; $C_{30}H$: C_{30}-hopane; GI: gammacerane/C_{30}-hopane; $C_{24}Te$: C_{24}-tetracyclic terpane; $C_{23}T$: C_{23}-tricyclic terpane.

https://doi.org/10.1021/acsomega.3c00273
ACS Omega 2023, 8, 16748−16761

Table 4. Parameters of Steranes (m/z 217) for Longtan Formation Shale Samples in Southern Anhui Province

	regular steranes (%)					
sample ID	C_{27}	C_{28}	C_{29}	C_{27}/C_{29}	C_{29} 20S/(20S + 20R)	C_{29} $\beta\beta/(\alpha\alpha + \beta\beta)$
CQ-8	36.38	26.62	37.00	0.98	0.44	0.45
CQ-6	36.30	26.58	37.13	0.98	0.41	0.44
CQ-4	35.51	26.60	37.89	0.94	0.42	0.41
DSC-6	36.14	25.31	38.55	0.94	0.39	0.46
DSC-4	38.55	26.57	34.88	1.11	0.44	0.47
DSC-2	43.73	24.57	31.70	1.38	0.47	0.49
GD-4	39.11	24.27	36.62	1.07	0.46	0.51
GD-3	38.48	24.76	36.76	1.05	0.39	0.42
GD-2	40.79	23.31	35.90	1.14	0.45	0.54
GD-1	42.32	23.66	34.02	1.24	0.41	0.47
average	38.73	25.23	36.05	1.08	0.43	0.47

ature.[22,32,43,44] In the present study, the relatively low GI values (0.16−0.27; average, 0.21; Table 3) found in all the samples indicate significant alterations due to maturity. Ratios of C_{31} 22S/(22S + 22R) hopane isomers vary from 0.41 to 0.60, with an average of 0.56 (Table 3), being close to the equilibrium value (0.60; Ji et al.[42]).

4.2.3. Steranes. The mass chromatograms of saturated hydrocarbons at m/z 217 reveal that steranes are predominantly composed of C_{27}, C_{28}, and C_{29} sterane homologues of regular steranes and diasteranes (Figure 5e−h), with low levels of pregnane series compounds. Table 4 presents the relative abundances of C_{27}, C_{28}, and C_{29} regular steranes, as well as the ratios of C_{27}/C_{29} regular steranes and the maturity biomarker indicators C_{29} 20S/(20S + 20R) and C_{29} $\beta\beta/(\alpha\alpha + \beta\beta)$. The relative proportion of C_{27} regular sterane is the highest (35.51%−43.73%, average: 38.73%), followed by C_{29} regular sterane (31.70%−38.55%, average: 36.05%), and C_{28} regular sterane (23.31%−26.62%, average: 25.23%). This indicates that the sterane belongs to the L-shaped distribution (Figure 5e−h). The ratios of C_{29} 20S/(20S + 20R) sterane isomers range from 0.39 to 0.47 (average, 0.43; Table 4), while those of C_{29} $\beta\beta/(\alpha\alpha + \beta\beta)$ sterane isomers are in the range of 0.41−0.54 (average, 0.47; Table 4), indicating high thermal maturity.[32]

4.2.4. $\delta^{13}C$ Values of Individual n-Alkanes. The $\delta^{13}C$ values of C_{15}−C_{32} n-alkanes for five rock samples range from −33.887% to −26.814‰, with an average of −30.213‰ (Table 5). Notably, the $\delta^{13}C$ compositions and values of individual n-alkanes differ among the samples from different sources. To be specific, the $\delta^{13}C$ values of C_{15}−C_{29} n-alkanes in two shale samples from the Gangdi-1 well range from −26.814% to −32.334‰ (average, −29.650‰), while the $\delta^{13}C$ values of C_{16}−C_{30} n-alkanes in two target samples from the Daoshanchong outcrop vary from −27.217% to 33.762‰ (average, −30.269‰). Additionally, the $\delta^{13}C$ values of C_{18}−C_{32} n-alkanes in one sample from the Changqiao outcrop vary from −28.604% to −33.887‰ (average, −31.230‰). Moreover, the $\delta^{13}C$ values of C_{15}−C_{32} n-alkanes within each sample vary by 3.5%−5.4‰ offset, with short-chain n-alkanes (<nC_{21}) displaying heavier $\delta^{13}C$ compositions than middle-chain (nC_{21}−nC_{25}) and long-chain n-alkanes (>nC_{25}) (Figure 6).

4.2.5. Mineralogical Compositions. Mineral compositions of siliceous rocks during their deposition and maturation are mainly indicative of the sedimentary environment and diagenetic evolution process. The Longtan Formation transitional shales are dominated by quartz and clay mineral with contents in the range of 32.5%−51.5% (average, 43.4%; Table 6) and 33.6%−48.1% (average, 41.5%; Table 6), respectively.

Table 5. $\delta^{13}C$ Values of C_{15}−C_{32} n-Alkanes for Five Rock Samples in Southern Anhui Province (‰ V-PDB)[a]

sample ID	GD-1	GD-3	DSC-2	DSC-4	CQ-4
nC_{15}	−27.299	−28.786	n.d	n.d	n.d
nC_{16}	−26.814	−28.821	−28.423	−27.574	n.d
nC_{17}	−28.361	−29.765	−28.757	−27.217	n.d
nC_{18}	−29.847	−30.087	−29.026	−27.902	−28.604
nC_{19}	−28.295	−30.714	−29.761	−28.568	−28.784
nC_{20}	−28.140	−30.211	−30.254	−28.081	−28.824
nC_{21}	−28.370	−30.051	−30.509	−28.783	−30.173
nC_{22}	−29.413	−30.541	−30.831	−29.084	−30.366
nC_{23}	−29.510	−31.539	−30.692	−29.587	−30.725
nC_{24}	−27.898	−30.739	−31.273	−30.262	−32.244
nC_{25}	−28.947	−31.292	−31.568	−30.734	−30.354
nC_{26}	−28.842	−31.723	−33.762	−31.342	−31.957
nC_{27}	−28.106	−31.127	−32.681	−31.874	−33.887
nC_{28}	−30.372	−32.334	−31.456	−32.117	−32.243
nC_{29}	−29.453	−32.103	−32.095	−31.094	−32.715
nC_{30}	n.d	n.d	−31.873	−30.875	−31.961
nC_{31}	n.d	n.d	n.d	n.d	−33.010
nC_{32}	n.d	n.d	n.d	n.d	−32.608
average	−28.644	−30.656	−30.864	−29.673	−31.230

[a]Note: n.d.: not determined.

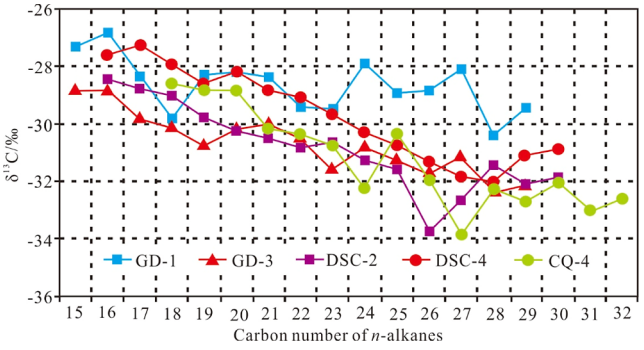

Figure 6. $\delta^{13}C$ values of C_{15}−C_{32} n-alkanes for Longtan Formation target samples from the Gangdi-1 well and two outcrops in Southern Anhui Province.

There are small amounts of calcite (average, 5.7%), pyrite (average, 5.5%), dolomite (average, 4.5%), and feldspar (average, 4.4%) (Table 6 and Figure 7a). Specifically, as illustrated in Figure 8, the Longtan transitional shale exhibits high clay mineral contents and low amounts of siliceous minerals (quartz and feldspar) relative to marine Woodford shale, Barnett

https://doi.org/10.1021/acsomega.3c00273
ACS Omega 2023, 8, 16748−16761

Table 6. Mineralogical Composition of Longtan Formation Shale in Southern Anhui Province

	mineral composition (%)						clay composition (%)			
sample ID	quartz	feldspar	calcite	dolomite	pyrite	clay	I/S	illite	kaolinite	chlorite
CQ-8	51.5	4.6	4.2		4.6	35.1	49	43	6	2
CQ-6	47.7	4.1	3.2		3.8	41.2	52	38	7	3
CQ-4	50.6		7.5	3.4	4.9	33.6	55	43	1	1
DSC-6	44.5		4.7	1.5	3.5	45.8	54	40	6	
DSC-4	48.7		4.8	2.1	3.8	40.6	40	53	4	3
DSC-2	46.5		4.6	1.9	4.2	42.8	61	35	2	2
GD-4	40.2		6.3	3.1	6.2	44.2	57	37	6	
GD-3	38.5			3.5	9.9	48.1	51	36	9	4
GD-2	33.3		12.1	4.9	9.2	40.5	66	26	8	
GD-1	32.5		4.2	15.6	5.3	42.4	62	38		
average	43.4	4.4	5.7	4.5	5.5	41.4	54.7	38.9	5.4	2.5

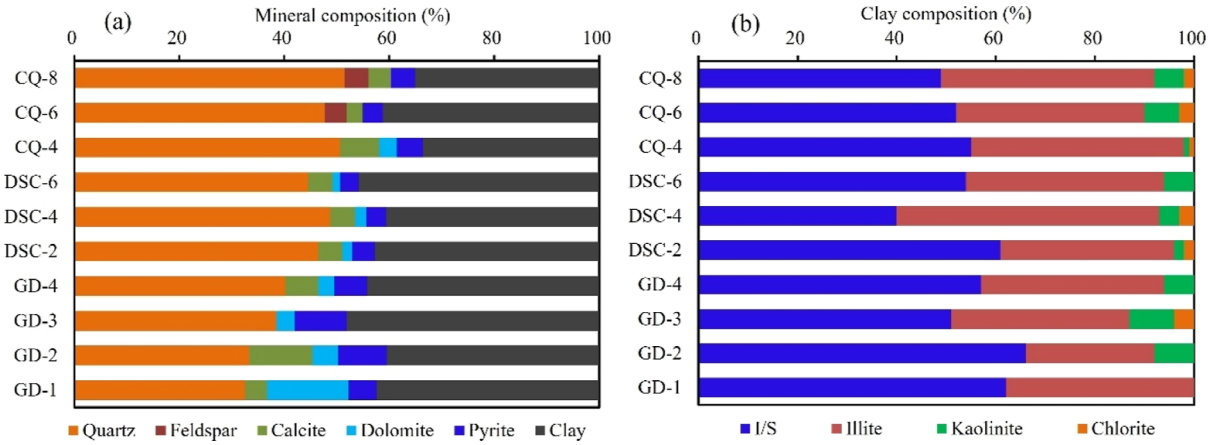

Figure 7. Mineralogical compositions of Longtan Formation transitional shale in Southern Anhui Province. (a) Mineral composition and (b) clay composition.

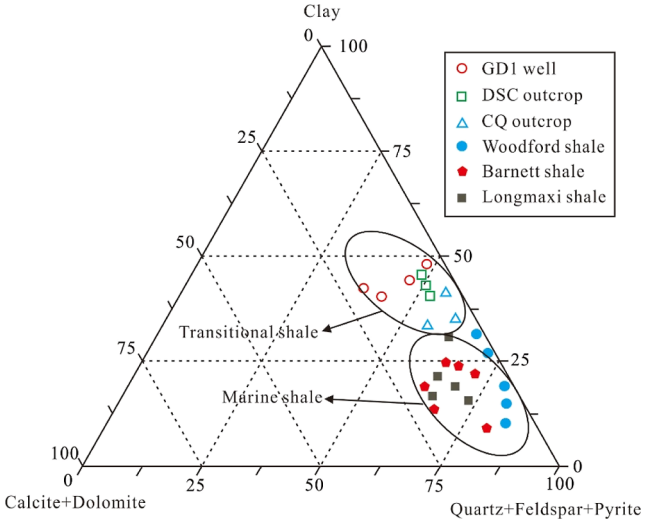

Figure 8. Ternary diagram of mineral compositions of Longtan Formation transitional shale (mineral compositions of Woodford, Barnett, and Longmaxi shales, adapted with permission from ref 46. Copyright 2017 Elsevier).

shale, and Longmaxi shale. The high clay contents of transitional shale would pose a challenge for shale gas development because of their low brittleness during hydrofracturing.

Furthermore, the Longtan Formation transitional shales contain a variety of clay minerals, including kaolinite, illite, illite−smectite (I/S) mixed clay, and chlorite. Based on the XRD testing results (Table 6 and Figure 7b), we can acquire that the predominant clay minerals are I/S and illite in Longtan Formation transitional shales with their weight percentages in the range of 40%−66% (average 54.7%) and 26%−53% (average 38.9%), respectively. Additionally, there are small amounts of kaolinite and chlorite averaging 5.4% and 2.5%, respectively. The transformation of clay minerals from kaolinite to illite, with I/S being an intermediate product, during the compaction indicates the diagenetic transformation process. This makes the clay mineral assemblage patterns useful for mirroring the diagenetic stage.[29,45] Particularly, the higher contents of I/S suggest that the Longtan Formation transitional shales are in the middle diagenetic stage B period.[45]

5. DISCUSSION

5.1. Organic Matter Sources. The relative distribution of *n*-alkanes and their $\delta^{13}C$ values are commonly used to determine the sources of organic matter.[26,38,44] Typically, the short-chain *n*-alkanes ($<nC_{21}$) mainly originated from bacteria and algae,[26,38,47,48] while the long-chain *n*-alkanes ($>nC_{25}$) are predominantly derived from higher plants on land.[48,49] The *n*-alkane patterns of the target samples display scattered carbon distributions (e.g., unimodal, bimodal, and multimodal) with the carbon peak in the range of nC_{15}−nC_{24} (Figure 4). Among them, the chromatograms for the target samples from the Daoshanchong outcrop and the Changqiao outcrop have carbon peaks ranging from nC_{19} to nC_{24} and relatively high quantities of

https://doi.org/10.1021/acsomega.3c00273
ACS Omega 2023, 8, 16748−16761

medium-chain *n*-alkanes ($nC_{22}-nC_{25}$) (Figure 4). This indicates that organic matter in Longtan Formation transitional shale is mostly derived from a mixed source of lower aquatic organisms and terrestrial higher plants, which may be the material basis for organic matter enrichment.

Besides, the terrigenous/aquatic ratio (TAR) is a useful tool not only for indicating biotic productivity levels (e.g., eutrophic and non-eutrophic waters) but also for qualitatively evaluating the relative contribution of terrestrial and aquatic sourced organic matter.[50] It is generally believed that high TAR values mean more abundant inputs of terrestrial higher plants from the surrounding water column relative to lower aquatic organisms.[38,50] To be specific, TAR values ≤1 typically represent eutrophic water and the dominance of aquatic sourced organic matter,[27,38,51] while TAR values >1 represent non-eutrophic systems and an increased proportion of terrestrial sourced organic matter.[27,38,50−52] The investigated samples have TAR values ranging from 0.23 to 2.46 (average 1.02, Table 2), probably implying that organic matter belongs to a mixed source of lower aquatic microbes and terrestrial higher plants.

Moreover, previous studies have demonstrated that the $\delta^{13}C$ values of individual *n*-alkanes with various carbon numbers are generally similar and variations of the *n*-alkane $\delta^{13}C$ values are typically less than 1.6‰ when organic matter origins are relatively uniform.[53,54] However, the $\delta^{13}C$ values of $C_{15}-C_{32}$ *n*-alkanes for the investigated samples in this study are in the range of 3.5‰−5.4‰ offset (Table 5), which is significantly higher than that (1.6‰) of *n*-alkanes from a single source. Additionally, the rock samples have variable $\delta^{13}C$ values with molecular weight (Figure 6), indicating the presence of at least two different organic matter sources.[53] This finding is consistent with the scenario inferred from TAR values as discussed above.

In addition, the relative concentrations of C_{27}, C_{28}, and C_{29} regular steranes are broadly used to distinguish organic matter sources.[55,56] Existing studies have shown that C_{29} regular steranes are associated with terrestrial higher plants, while C_{27} regular steranes are primarily derived from aquatic planktons or algae.[44,56−58] As a result, ratios of C_{27}/C_{29} regular steranes are a reliable biomarker indicator for evaluating the relative contributions of terrestrial and aquatic organic matter.[38,56] Medium ratios of C_{27}/C_{29} regular steranes (0.94−1.38, average: 1.08; Table 4) elucidate that Longtan Formation shales were dominated by a mixed source of aquatic and terrestrial organic matter as indicated by the ternary diagram of $C_{27}-C_{28}-C_{29}$ regular steranes (Figure 9). Furthermore, the high abundance of tricyclic terpanes relative to tetracyclic terpanes, represented by relatively low C_{24}-tetracyclic/C_{23}-tricyclic ratios ($C_{24}Te/C_{23}T$; Table 3), is assigned to a high contribution of aquatic organic matter.

5.2. Thermal Maturity. R_o is a widely used proxy for assessing the quality of black shale and its thermal maturity. The Longtan Formation shale exhibits moderate R_o values ranging from 1.23% to 1.63% (average, 1.41%; Table 1), indicating that organic matter has reached the mature stage of hydrocarbon generation. In addition to R_o, T_{max} is another critical indicator of thermal maturity. Threshold values of 435, 470, and 490 °C are commonly used to differentiate oil window, wet gas window, and dry gas window, respectively.[32,36] The Longtan Formation rock samples have T_{max} values ranging from 435 to 496 °C (average, 461 °C; Table 1), which confirms that Longtan Formation's organic matter enrichment has been thermally matured and suggests that it falls within the wet gas window. It is worth noting that the R_o and T_{max} values exhibit no significant fluctuations in the Longtan interval, indicating a consistent thermal evolution of organic matter in Longtan Formation shale.

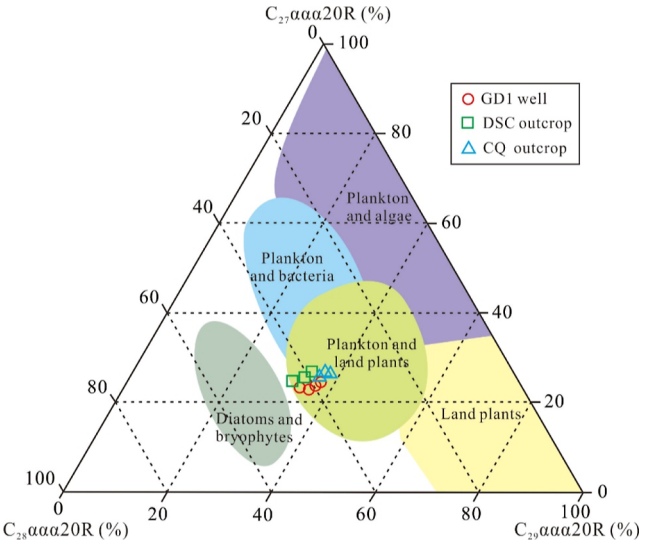

Figure 9. Ternary diagram of $C_{27}-C_{28}-C_{29}$ regular steranes of Longtan Formation shale samples from the Gangdi-1 (GD1) well, Daoshanchong (DSC) outcrop, and Changqiao (CQ) outcrop (base map adapted with permission from ref 44. Copyright 2016 Elsevier).

Biomarker indicators, such as ratios of C_{31} 22S/(22S + 22R), C_{29} 20S/(20S + 20R), and C_{29} $\beta\beta/(\alpha\alpha + \beta\beta)$, are also widely used to evaluate the organic matter maturity.[27,32,38,55] The equilibrium value of C_{31} 22S/(22S + 22R) ratio is in the range of 0.57−0.62.[27] Ratios of C_{31} 22S/(22S + 22R) hopane of the target samples range from 0.41 to 0.60 (average, 0.56; Table 3) and have essentially reached the equilibrium range, reflecting that organic matter has reached the mature stage of hydrocarbon generation.[32,59] Furthermore, ratios of C_{29} 20S/(20S + 20R) sterane and C_{29} $\beta\beta/(\alpha\alpha + \beta\beta)$ sterane increase with increasing thermal maturity.[11,26,60] The investigated samples have C_{29} 20S/(20S + 20R) and C_{29} $\beta\beta/(\alpha\alpha + \beta\beta)$ ratios in the ranges of 0.39−0.47 and 0.41−0.54, respectively, supporting the conclusion that the Longtan Formation shale has reached the mature stage of hydrocarbon generation.

5.3. Palaeoredox Condition. *5.3.1. Constraints from Cross plot of TOC versus TS.* The correlation between TOC and TS contents is a useful tool for characterizing the palaeoredox conditions. This is based on the relationship between organic matter decomposition and the formation of sulfur in pyrite. The Longtan Formation shales primarily consist of quartz and clay minerals with minor amounts of calcite, pyrite, dolomite, and feldspar (Figure 7a). Sulfur mainly exists in pyrite, and the formation of pyrite is closely associated with the decomposition of organic matter. Previous studies have shown that a clear positive relationship between TOC and TS contents with a zero or close to zero intercept indicates normal marine oxic conditions.[35,61] Conversely, no significant positive relationship between TOC and TS contents probably reflects anoxic or euxinic conditions.

As shown in Figure 10, there is an obvious positive correlation between TOC and TS contents (R^2 = 0.90 in the TOC−TS diagram), with an intercept of 0.54 on the TS coordinate axis. These results suggest that the sulfur enrichment in Longtan Formation transitional shales was strongly influenced by the availability of unstable organic carbon. Most of the investigated samples display relatively low TS content (average, 1.26%; Table

https://doi.org/10.1021/acsomega.3c00273
ACS Omega 2023, 8, 16748−16761

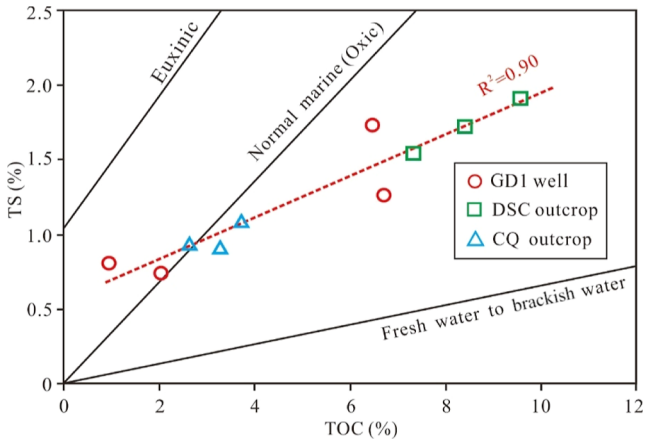

Figure 10. Cross plot of TOC vs TS contents for Longtan Formation shale samples from the Gangdi-1 (GD1) well, Daoshanchong (DSC) outcrop, and Changqiao (CQ) outcrop.

1), which suggests that the emergence of pyrite was primarily limited by the supply of sulfides (e.g., H_2S or HS^-) rather than reactive iron.[28,34,35] Taken together, these results indicate that the water column was likely in an oxidized state during Longtan Formation shale deposition.

5.3.2. Constraints from Biomarkers. The Pr/Ph ratio is extensively used to indicate the palaeoredox conditions.[26,32,38,40] For instance, a high Pr/Ph ratio (>3.0) is generally indicative of organic matter deposited in oxic conditions,[32] while a low Pr/Ph ratio (<1.0) frequently indicates anoxic conditions, and an intermediate Pr/Ph ratio in the range of 1.0−3.0 normally suggests dysoxic conditions.[26,62] In this study, Pr/Ph ratios of the target samples range from 0.96 to 1.85 (average, 1.36; Table 2), deciphering that Longtan Formation transitional shales were mainly deposited in a dysoxic water environment. Moreover, the plot of Pr/nC_{17} vs Ph/nC_{18} (Figure 11) also suggests a

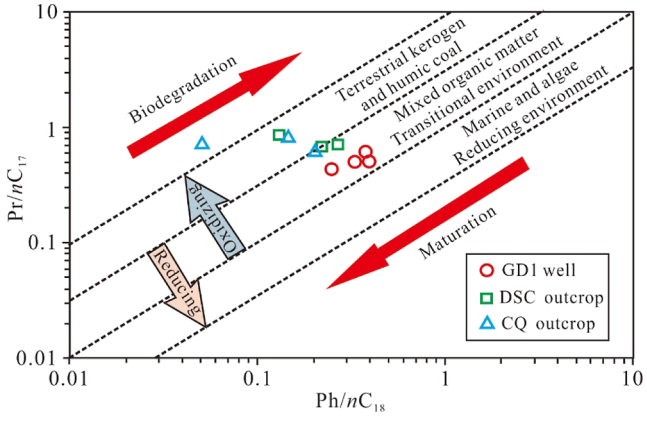

Figure 11. Plot of Pr/nC_{17} vs Ph/nC_{18} of Longtan Formation rock samples from the Gangdi-1 (GD1) well, Daoshanchong (DSC) outcrop, and Changqiao (CQ) outcrop (base map adapted with permission from ref 28. Copyright 2020 Elsevier).

transitional (dysoxic-to-oxic) condition, being consistent with the conclusion inferred from previously published trace element paleoredox proxies.[15] Additionally, the *n*-alkane distributions, which peak at even carbon numbers (Table 2), further support the inference of dysoxic or oxic conditions.[63,64]

5.3.3. Constraints from Pyrite Morphology. Pyrite framboid diameter has been proven to be one of the practical tools to determine the paleoredox conditions.[65−68] Existing studies have illustrated that the diameters of pyrite framboids developed in anoxic water environments are smaller on average and relatively stable in size than those formed in oxic or dysoxic bottom waters.[68] In this study, scanning electron microscopy (SEM) examination of a total of eight shale samples reveals that variable pyrite morphologies are present, mainly including normal framboids (Figure 12a−d), clustered framboids (Figure 12c), partially recrystallized framboids (Figure 12e), and irregular anhedral to subhedral pyrites (Figure 12f). Framboid diameter mean values are in the range of 7.04−8.30 μm (average, 7.62 μm; Table 7), which is clearly higher than the corresponding values of the pyrite framboids formed in anoxic water columns (4.7 ± 0.5 μm; Wilkin et al.[66]) and basically comparable to that of pyrite framboids developed in oxic or dysoxic bottom waters (7.7 ± 4.1 μm; Wilkin et al.[66]). Moreover, the majority of maximum framboid diameter (MFD) values were greater than 12.0 μm (Table 7), indicating a longer residence time for their growth that could not have occurred in anoxic or euxinic porewater conditions.[65,68] These observations together suggest that the pyrite framboids in the Longtan interval were likely formed in oxic or dysoxic water columns.

Furthermore, cross plots of the mean size of framboids versus standard deviation (Figure 13a) and skewness (Figure 13b) show that all the pyrite framboids formed in a dysoxic-to-oxic environment, being consistent with the scenario inferred from the data of MFD as documented above. Framboids are generally absent in fully oxic conditions.[68,69] Accordingly, we speculated that the dysoxic-to-oxic conditions of water columns developed during transitional shale deposition.

5.4. Depositional Models of Organic Matter Enrichment. During the Late Permian, the Longtan Formation in Southern Anhui Province is divided into three components: the lower and upper intervals are believed to form in a delta sedimentary system, while the middle interval is thought to develop in a tidal flat-lagoon system.[7] Through analysis of biomarker distributions and pyrite morphology, organic matter sources and palaeoredox conditions are deciphered across the Longtan interval. Based on these analyses, depositional models of organic matter enrichment in such a setting are established (Figure 14a,b).

Previous studies have revealed that Southern Anhui Province experienced a warm and humid climate during the Longtan period based on published paleoclimate proxies.[12] This favorable climate promoted the growth of terrestrial higher plants and accelerated the chemical weathering degree of parent rocks, resulting in increased nutrients in the water column that facilitated the mass reproduction of bacteria and phytoplanktons. Therefore, a mixed source of terrestrial higher plants and lower aquatic organisms may constitute the material basis for organic matter accumulation and contribute to increased primary productivity in Longtan Formation. In addition, the sedimentary rate also plays a significant role in organic matter accumulation.[19,67,70] A high sedimentary rate is usually favorable for organic matter accumulation under an oxic environment, as the rapid burial can shorten the exposure time of organic matter to the oxidized water column.[19,70,71] Conversely, a high sedimentary rate can lead to organic matter dilution and is unfavorable for organic matter preservation in a reducing environment.[16,19,72] Although the dysoxic-to-oxic water environment during transitional shale deposition in Southern Anhui Province is not conducive to organic matter preservation, a higher sedimentation rate elucidated by previously published

https://doi.org/10.1021/acsomega.3c00273
ACS Omega 2023, 8, 16748−16761

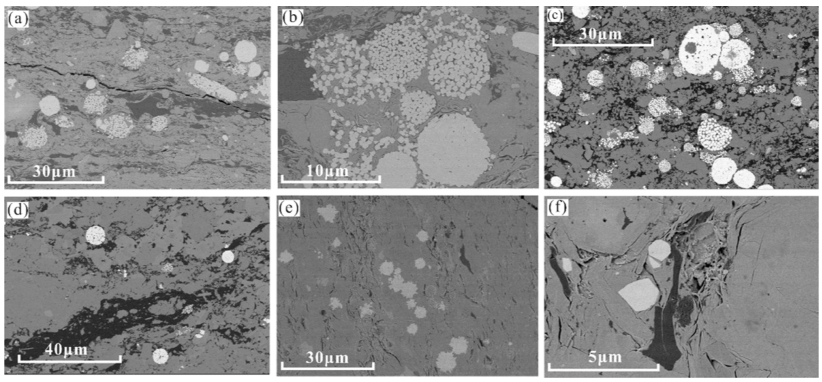

Figure 12. SEM photomicrographs of pyrite morphology. (a) Normal framboids and columnar pyrite, GD-1; (b) normal framboids and loose aggregation of microcrystals, GD-3; (c) clustered framboids showing different sizes of microcrystals, DSC-2; (d) normal framboids showing uniform microcrystals, CQ-4; (e) partially recrystallized framboids, GD-2; (f) irregular anhedral to subhedral pyrite crystals, GD-4.

Table 7. Pyrite Content and Statistics of Framboid Size for Longtan Formation Shale Samples in Southern Anhui Province[a]

sample ID	framboidal pyrite (%)	mean (μm)	MFD (μm)	standard deviation (μm)	skewness	number
CQ-6	48.2	7.74	16.72	3.90	0.76	35
CQ-4	51.9	7.91	13.25	2.72	0.30	28
DSC-4	45.3	7.54	14.48	2.72	0.87	35
DSC-2	49.4	7.06	12.54	3.10	0.15	42
GD-4	34.1	8.30	14.72	3.00	0.72	36
GD-3	52.8	7.74	16.70	3.40	0.97	45
GD-2	39.1	7.04	15.41	3.28	1.06	32
GD-1	45.7	7.60	12.19	2.50	0.33	35
average	45.8	7.62	14.50	3.08	0.64	38

[a]MFD: maximum framboid diameter.

trace element proxies (e.g., Liu et al.[15] and Wu et al.[12]) tends to decrease organic matter decomposition in the oxidized water column, resulting in the preservation of a substantial amount of organic matter through rapid burial.[19]

6. CONCLUSIONS

Based on the analyses of organic geochemistry, mineral composition, and pyrite morphology of Longtan Formation rock samples from the Gangdi-1 well, Daoshanchong outcrop, and Changqiao outcrop, the following conclusions can be made:

(1) The chromatograms exhibit unimodal, bimodal, and multimodal distributions with the carbon peak in the range of nC$_{15}$−nC$_{24}$, combined with the variations of δ^{13}C values of C$_{13}$−C$_{26}$ n-alkanes and the ternary diagram of C$_{27}$−C$_{28}$−C$_{29}$ regular steranes together suggest that organic matter in Longtan Formation black shale may have originated from the mixed sources of lower aquatic organisms and terrestrial higher plants.

(2) The organic matter in Longtan Formation shale has reached the mature stage of hydrocarbon generation, as evidenced by thermal proxies, such as organic petrography (R_o and T_{max}) and biomarkers (ratios of C$_{31}$ 22S/(22S + 22R), C$_{29}$ 20S/(20S + 20R), and C$_{29}$ $\beta\beta$/($\alpha\alpha$ + $\beta\beta$)).

(3) Cross plot of TOC vs TS and Pr/nC$_{17}$ vs Ph/nC$_{18}$ diagram, along with the Pr/Ph ratio and pyrite morphology, suggest that Longtan Formation transitional shales were primarily deposited in a dysoxic-to-oxic water environment.

(4) Depositional models of organic matter accumulation in deltaic and tidal flat-lagoon systems are proposed. For one thing, the abundant mixed sourced organic matters can directly contribute to enhancing the primary productivity. For another, a higher sedimentation rate can significantly reduce the exposure time of organic matter in the dysoxic-to-oxic water environment, leading to the preservation of a substantial amount of organic matter through rapid burial.

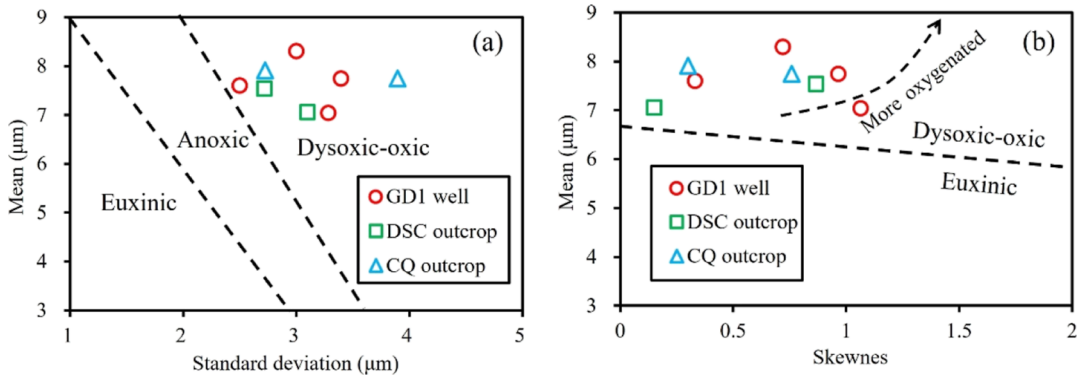

Figure 13. Cross plots of (a) mean vs standard deviation and (b) skewness of the framboid size (base map adapted with permission from ref 68. Copyright 2016 Elsevier).

https://doi.org/10.1021/acsomega.3c00273
ACS Omega 2023, 8, 16748−16761

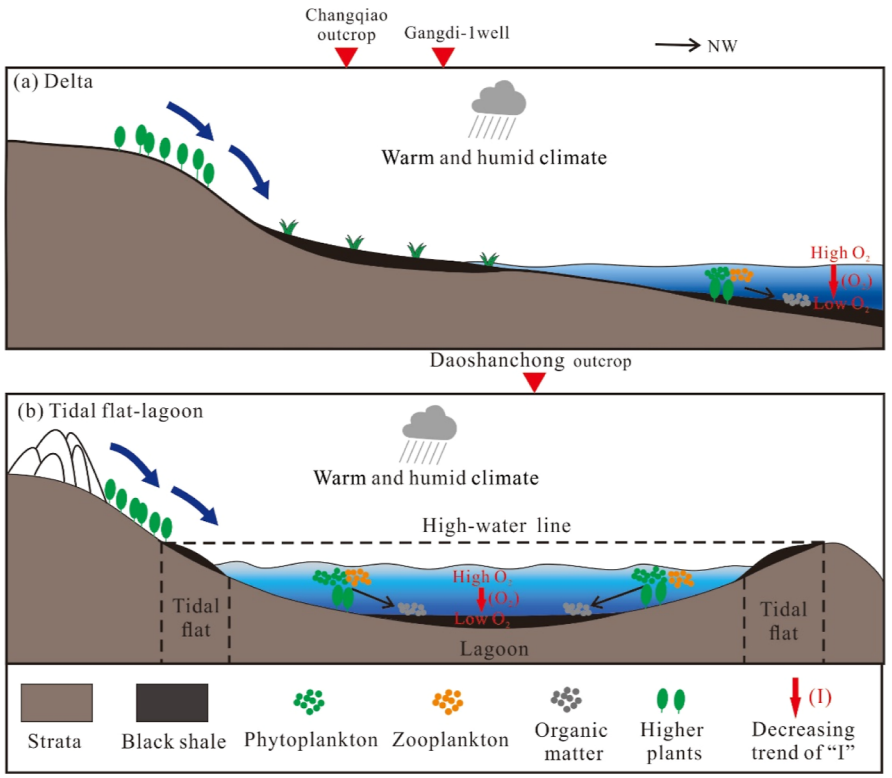

Figure 14. Depositional models of organic matter accumulation for Longtan Formation transitional shale.

AUTHOR INFORMATION

Corresponding Authors

Jianghui Ding − *CNPC Engineering Technology R & D Company Limited, Beijing 102206, People's Republic of China; PetroChina Research Institute of Petroleum Exploration and Development, Beijing 100083, People's Republic of China;* orcid.org/0000-0002-5563-628X; Email: djhdream2015@163.com

Haikuan Nie − *State Key Laboratory of Shale Oil and Gas Enrichment Mechanisms and Effective Development, Beijing 102206, People's Republic of China; Sinopec Petroleum Exploration and Production Research Institute, Beijing 102206, People's Republic of China;* orcid.org/0000-0002-3634-1523; Email: niehk.syky@sinopec.com

Authors

Jinsheng Sun − *CNPC Engineering Technology R & D Company Limited, Beijing 102206, People's Republic of China*

Xiangtong Yang − *CNPC Engineering Technology R & D Company Limited, Beijing 102206, People's Republic of China*

Yu Ye − *CNPC Engineering Technology R & D Company Limited, Beijing 102206, People's Republic of China*

Gang Shi − *Nanjing Center of China Geological Survey, Nanjing, Jiangsu 210061, People's Republic of China*

Ruyi Wang − *CNPC Engineering Technology R & D Company Limited, Beijing 102206, People's Republic of China*

Bo Huang − *CNPC Engineering Technology R & D Company Limited, Beijing 102206, People's Republic of China*

Xun Sun − *CNPC Engineering Technology R & D Company Limited, Beijing 102206, People's Republic of China*

Huili Li − *CNPC Engineering Technology R & D Company Limited, Beijing 102206, People's Republic of China*

Complete contact information is available at: https://pubs.acs.org/10.1021/acsomega.3c00273

Notes

The authors declare no competing financial interest.

ACKNOWLEDGMENTS

The authors would like to thank the funding support from the Major Science and Technology Project of China National Petroleum Corporation (2020F-50, 2021DJ4504, and 2021ZZ10-05). The authors also appreciate the Nanjing Center of China Geological Survey for providing access to core samples.

REFERENCES

(1) Tan, J.; Horsfield, B.; Fink, R.; Krooss, B.; Schulz, H.; Rybacki, E.; Zhang, J. C.; Boreham, C. J.; van Graas, G.; Tocher, B. A. Shale gas potential of the major marine shale formations in the upper Yangtze platform, South China, Part III: mineralogical, lithofacial, petrophysical, and rock mechanical properties. *Energy Fuels* **2014**, *28*, 2322−2342.

(2) Dang, W.; Zhang, J. C.; Tang, X.; Chen, Q.; Han, S. B.; Li, Z. M.; Du, X. R.; Wei, X. L.; Zhang, M. Q.; Liu, J.; Peng, J. L.; Huang, Z. L. Shale gas potential of Lower Permian marine-continental transitional black shales in the Southern North China Basin, central China: Characterization of organic geochemistry. *J. Nat. Gas Sci. Eng.* **2016**, *28*, 639−650.

(3) Nie, H. K.; Jin, Z. J.; Sun, C. X.; He, Z. L.; Liu, G.; Liu, Q. Y. Organic Matter Types of the Wufeng and Longmaxi Formations in the Sichuan Basin, South China: Implications for the Formation of Organic Matter Pores. *Energy Fuels* **2019**, *33*, 8076−8100.

(4) Zou, C. N.; Zhu, R. K.; Chen, Z. Q.; Ogg, J. G.; Wu, S. T.; Dong, D. Z.; Qiu, Z.; Wang, Y. M.; Wang, L.; Lin, S. H.; Cui, J. W.; Su, L.; Yang, Z. Organic matter rich shales of China. *Earth-Sci. Rev.* **2019**, *189*, 51−78.

(5) Zhang, J. C.; Tao, J.; Li, Z.; Wang, X. W.; Li, X. Q.; Jiang, S. L.; Wang, D. S.; Zhao, X. X. Prospect of deep shale gas resources in China. *Nat. Gas Ind.* **2021**, *41*, 15−28.

(6) Liao, Z. W.; Hu, W. X.; Cao, J.; Wang, X. L.; Hu, Z. Y. Petrologic and geochemical evidence for the formation of organic-rich siliceous rocks of the Late Permian Dalong Formation, Lower Yangtze region, southern China. *Mar. Pet. Geol.* **2019**, *103*, 41−54.

(7) Du, X. B.; Song, X. D.; Zhang, M. Q.; Lu, Y. C.; Lu, Y. B.; Chen, P.; Liu, Z. H.; Yang, S. Shale gas potential of the lower permian gufeng formation in the western area of the lower Yangtze platform, China. *Mar. Pet. Geol.* **2015**, *67*, 526−543.
(8) Xie, X. M.; Li, M. W.; Littke, R.; Huang, Z. K.; Ma, X. X.; Jiang, Q. G.; Snowdon, L. R. Petrographic and geochemical characterization of microfacies in a lacustrine shale oil system in the Dongying Sag, Jiyang Depression, Bohai Bay Basin, eastern China. *Int. J. Coal Geol.* **2016**, *165*, 49−63.
(9) Liang, D. G.; Guo, T. L.; Chen, J. P.; Bian, L. Z.; Zhao, Z. Some progresses on studies of hydrocarbon generation and accumulation in marine sedimentary regions, Southern China (part 2): Geochemical characteristics of four suits of regional marine source rocks, South China. *Mar. Petrol. Geol.* **2009**, *14*, 1−15.
(10) Cai, C. F.; Xiang, L.; Yuan, Y. Y.; Xu, C. L.; He, W. X.; Tang, Y. J.; Borjigin, T. Sulfur and carbon isotopic compositions of the Permian to Triassic TSR and non-TSR altered solid bitumen and its parent source rock in NE Sichuan Basin. *Org. Geochem.* **2017**, *105*, 1−12.
(11) Zhang, J. Z.; Li, X. Q.; Zhang, X. Q.; Zhang, M.; Cong, G. S.; Zhang, G. W.; Wang, F. Y. Geochemical and geological characterization of marine-continental transitional shales from Longtan Formation in Yangtze area, South China. *Mar. Pet. Geol.* **2018**, *96*, 1−15.
(12) Wu, Z. R.; He, S.; He, Z. L.; Li, X. C.; Zhai, G. Y.; Huang, Z. Q. Petrographical and geochemical characterization of the Upper Permian Longtan formation and Dalong Formation in the Lower Yangtze region, South China: Implications for provenance, paleoclimate, paleoenvironment and organic matter accumulation mechanisms. *Mar. Pet. Geol.* **2022**, *139*, 105580.
(13) Ding, J. H.; Zhang, J. C.; Huo, Z. P.; Shen, B. J.; Shi, G.; Yang, Z. H.; Li, X. Q.; Li, C. X. Controlling factors and formation models of organic matter accumulation for the Upper Permian Dalong Formation black shale in the Lower Yangtze region, South China: Constraints from geochemical evidence. *ACS Omega* **2021**, *6*, 3681−3692.
(14) Huang, B. G.; Shi, R. F.; Zhao, X. B.; Zhou, G. Geological conditions of Paleozoic shale gas formation and its exploration potential in the South Anhui, Lower Yangtze area. *J. China Coal Soc.* **2013**, *38*, 877−882.
(15) Liu, S. X.; Wu, C. F.; Li, T.; Wang, H. C. Multiple geochemical proxies controlling the organic matter accumulation of the marine-continental transitional shale: A case study of the Upper Permian Longtan Formation, western Guizhou, China. *J. Nat. Gas Sci. Eng.* **2018**, *56*, 152−165.
(16) Arthur, M. A.; Sageman, B. B. Marine black shales: Depositional mechanisms and environments of ancient deposits. *Annu. Rev. Earth Planet Sci.* **1994**, *22*, 499−551.
(17) Wei, H. Y.; Chen, D. Z.; Wang, J. G.; Yu, H.; Tucker, M. E. Organic accumulation in the lower Chihsia Formation (Middle Permian) of South China: Constraints from pyrite morphology and multiple geochemical proxies. *Palaeogeogr. Palaeoclimatol. Palaeoecol.* **2012**, *353*−*355*, 73−86.
(18) Ding, J.; Sun, J.; Nie, H. K.; Yang, X. T.; Ye, Y.; Shi, G.; Wang, R. Y.; Huang, B.; Li, H. L. Application of biomarkers in characterization of organic matter source, maturity and palaeoredox condition of black shales from the upper Permian Dalong Formation in Southern Anhui Province, South China. *Geol. J.* **2023**, *58*, 1−19.
(19) Cao, J.; Yang, R. F.; Yin, W.; Hu, G.; Bian, L. Z.; Fu, X. G. Mechanism of organic matter accumulation in residual bay environments: The Early Cretaceous Qiangtang Basin. Tibet. *Energy Fuels* **2018**, *32*, 1024−1037.
(20) Wang, E. Z.; Guo, T. L.; Li, M. W.; Xiong, L.; Dong, X. X.; Zhang, N. X.; Wang, T. Depositional environment variation and organic matter accumulation mechanism of marine−continental transitional shale in the upper Permian Longtan Formation, Sichuan Basin, SW China. *ACS Earth Space Chem.* **2022**, *6*, 2199−2214.
(21) Luo, W.; Hou, M. C.; Liu, X. C.; Huang, S. G.; Chao, H.; Zhang, R.; Deng, X. Geological and geochemical characteristics of marine-continental transitional shale from the upper permian longtan formation, Northwestern Guizhou, China. *Mar. Pet. Geol.* **2018**, *89*, 58−67.
(22) ten Haven, H. L.; de Leeuw, J. W.; Rullkötter, J.; Damsté, J. S. S. Restricted utility of the pristane/phytane ratio as a palaeoenvironmental indicator. *Nature* **1987**, *330*, 641−643.
(23) Freeman, K. H.; Hayes, J. M.; Trendel, J. M.; Albrecht, P. Evidence from carbon isotope measurements for diverse origins of sedimentary hydrocarbons. *Nature* **1990**, *343*, 254−256.
(24) Schwark, L.; Empt, P. Sterane biomarkers as indicators of palaeozoic algal evolution and extinction events. *Palaeogeogr. Palaeoclimatol. Palaeoecol.* **2006**, *240*, 225−236.
(25) Hao, F.; Zhou, X.; Zhu, Y.; Yang, Y. Mechanisms for oil depletion and enrichment on the Shijiutuo Uplift, Bohai Bay Basin, China. *AAPG Bull.* **2009**, *93*, 1015−1037.
(26) Sarki Yandoka, B. M.; Abdullah, W. H.; Abubakar, M. B.; Hakimi, M. H.; Adegoke, A. K. Geochemical characterisation of Early Cretaceous lacustrine sediments of Bima Formation, Yola Sub-basin, Northern Benue Trough, NE Nigeria: Organic matter input, preservation, paleoenvironment and palaeoclimatic conditions. *Mar. Pet. Geol.* **2015**, *61*, 82−94.
(27) Caro Gonzalez, L. D.; Mastalerz, M.; Filho, J. G. M. Application of organic facies and biomarkers in characterization of paleoenvironmental conditions and maturity of sediments from the Codó Formation in the west-central part of the São Luís Basin, Brazil. *Int. J. Coal Geol.* **2020**, *225*, 103482.
(28) Mansour, A.; Geršlová, E.; Sýkorová, I.; Vöröš, D. Hydrocarbon potential and depositional paleoenvironment of a Middle Jurassic succession in the Falak-21 well, Shushan Basin, Egypt: Integrated palynological, geochemical and organic petrographic approach. *Int. J. Coal Geol.* **2020**, *219*, 103374.
(29) Ding, J. H.; Zhang, J. C.; Tang, X.; Huo, Z. P.; Han, S. B.; Lang, Y.; Zheng, Y. Y.; Li, X. Q.; Liu, T. Elemental geochemical evidence for depositional conditions and organic matter enrichment of black rock series strata in an inter-platform basin: The Lower Carboniferous Datang Formation, Southern Guizhou, Southwest China. *Minerals* **2018**, *8*, 509.
(30) Schoenherr, J.; Littke, R.; Urai, J. L.; Kukla, P. A.; Rawahi, Z. Polyphase thermal evolution in the Infra-Cambrian Ara Group (South Oman Salt Basin) as deduced by maturity of solid reservoir bitumen. *Org. Geochem.* **2007**, *38*, 1293−1318.
(31) Carvajal-Ortiz, H.; Gentzis, T. Critical considerations when assessing hydrocarbon plays using Rock-Eval pyrolysis and organic petrology data: Data quality revisited. *Int. J. Coal Geol.* **2015**, *152*, 113−122.
(32) Peters, K. E.; Walters, C. C.; Moldowan, J. M. *The Biomarker Guide: Biomarkers and Isotopes in Petroleum Exploration and Earth History*, 2nd ed.; Cambridge University Press: Cambridge, 2005; Vol. 2.
(33) Yang, S. Y.; Schulz, H. M. Factors controlling the petroleum generation characteristics of Palaeogene source rocks in the Austrian Molasse Basin as revealed by principal component analysis biplots. *Mar. Pet. Geol.* **2019**, *99*, 323−336.
(34) Beier, J. A.; Hayes, J. M. Geochemical and isotopic evidence for paleoredox conditions during deposition of the Devonian-Mississippian New Albany Shale, Southern Indiana. *Geol. Soc. Am. Bull.* **1989**, *101*, 774−782.
(35) Berner, R. A.; Raiswell, R. Burial of organic carbon and pyrite sulfur in sediments over Phanerozoic time: A new theory. *Geochem. Cosmochim. Acta* **1983**, *47*, 855−862.
(36) Espitalié, J.; Deroo, G.; Marquis, F. La pyrolyse Rock-Eval et ses applications. Troisième partie. *Inst. Fr. Pet.* **1986**, *41*, 73−89.
(37) Wang, B.; Yang, J.; Jiang, H.; Zhang, G.; Dong, H. Chemical composition of n-alkanes and microbially mediated n-alkane degradation potential differ in the sediments of Qinghai-Tibetan lakes with different salinity. *Chem. Geol.* **2019**, *524*, 37−48.
(38) Kong, X. X.; Jiang, Z. X.; Zheng, Y. H.; Xiao, M.; Chen, C.; Yuan, H.; Chen, F. L.; Wu, S. Q.; Zhang, J. G.; Han, C.; Liu, S. Q. Organic geochemical characteristics and organic matter enrichment of mudstones in an Eocene saline lake, Qianjiang Depression, Hubei Province, China. *Mar. Pet. Geol.* **2020**, *114*, 104194.
(39) Flannery, E. N.; George, S. C. Assessing the syngeneity and indigeneity of hydrocarbons in the 1.4 Ga Velkerri Formation, Mc

https://doi.org/10.1021/acsomega.3c00273
ACS Omega 2023, 8, 16748−16761

Arthur Basin, using slice experiments. *Org. Geochem.* **2014**, *77*, 115−125.
(40) Powell, T. G.; Mc Kirdy, D. M. Relationship between ratio of pristane to phytane, crude oil composition and geological environment in Australia. *Nature* **1973**, *243*, 37−39.
(41) Hughes, W. B.; Holba, A. G.; Dzou, L. I. The ratios of dibenzothiophene to phenanthrene and pristane to phytane as indicators of depositional environment and lithology of petroleum source rocks. *Geochem. Cosmochim. Acta* **1995**, *59*, 3581−3598.
(42) Ji, W. M.; Hao, F.; Song, Y.; Tian, J. Q.; Meng, M. M.; Huang, H. X. Organic geochemical and mineralogical characterization of the lower Silurian Longmaxi shale in the southeastern Chongqing area of China: Implications for organic matter accumulation. *Int. J. Coal Geol.* **2020**, *220*, 103412.
(43) Sinninghe Damsté, J. S.; Kenig, F.; Koopmans, M. P.; Köster, J.; Schouten, S.; Hayes, J. M.; de Leeuw, J. W. Evidence for gammacerane as an indicator of water column stratification. *Geochem. Cosmochim. Acta* **1995**, *59*, 1895−1900.
(44) Hakimi, M. H.; Abdullah, W. H.; Alqudah, M.; Makeen, Y. M.; Mustapha, K. A. Organic geochemical and petrographic characteristics of the oil shales in the Lajjun area, Central Jordan: Origin of organic matter input and preservation conditions. *Fuel* **2016**, *181*, 34−45.
(45) Yang, C.; Zhang, J. C.; Tang, X.; Ding, J. H.; Zhao, Q. R.; Dang, W.; Chen, H. Y.; Su, Y.; Li, B. W.; Lu, D. F. Comparative study on micro-pore structure of marine, terrestrial, and transitional shales in key areas, China. *Int. J. Coal Geol.* **2017**, *171*, 76−92.
(46) Xu, Q. L.; Liu, B.; Ma, Y. S.; Song, X. M.; Wang, Y. J.; Chen, Z. X. Geological and geochemical characterization of lacustrine shale: A case study of the Jurassic Da'anzhai member shale in the central Sichuan Basin, southwest China. *J. Nat. Gas Sci. Eng.* **2017**, *47*, 124−139.
(47) Gelpi, E.; Schneider, H.; Mann, J.; Oro, J. Hydrocarbons of geochemical significance in microscopic algae. *Phytochemistry* **1970**, *9*, 603−612.
(48) Mello, M. R.; Koutsoukos, E.; Hart, M. B.; Brassell, S. C.; Maxwell, J. R. Late cretaceous anoxic events in the Brazilian continental margin. *Org. Geochem.* **1989**, *14*, 529−542.
(49) Moldowan, J. M.; Seifert, W. K.; Gallegos, E. J. Relationship between petroleum composition and depositional environment of petroleum source rocks. *AAPG Bull.* **1985**, *69*, 1255−1268.
(50) Bourbonniere, R. A.; Meyers, P. A. Sedimentary geolipid records of historical changes in the watersheds and productivities of Lakes Ontario and Erie. *Limnol. Oceanogr.* **1996**, *41*, 352−359.
(51) Meyers, P. A. Organic geochemical proxies of paleoceanographic, paleolimnologicand paleoclimatic processes. *Org. Geochem.* **1997**, *27*, 213−250.
(52) Routh, J.; Choudhary, P.; Meyers, P. A.; Kumar, B. A sediment record of recent nutrient loading and trophic state change in lake Norrviken, Sweden. *J. Paleolimnol.* **2008**, *42*, 325−341.
(53) Xu, H. Y.; Hou, D. J.; LÖhr, S. C.; Liu, Q. Y.; George, S. C. Early diagenetic pyrite cementation influences molecular composition of sedimentary organic matter in the Dongying Depression, China. *Org. Geochem.* **2020**, *144*, 104019.
(54) Monson, K. D.; Hayes, J. M. Biosynthetic control of the natural abundance of carbon 13 at specific positions within fatty acids in Saccharomyces cerevisiae: Isotopic fractionation in lipid synthesis as evidence for peroxisomal regulation. *J. Biol. Chem.* **1982**, *257*, 5568−5575.
(55) Seifert, W. K.; Michael Moldowan, J. Applications of steranes, terpanes and monoaromatics to the maturation, migration and source of crude oils. *Geochem. Cosmochim. Acta* **1978**, *42*, 77−95.
(56) Huang, W. Y.; Meinschein, W. G. Sterols as ecological indicators. *Geochem. Cosmochim. Acta* **1979**, *43*, 739−745.
(57) Hartmann, M. A. Plant sterols and the membrane environment. *Trends Plant Sci.* **1998**, *3*, 170−175.
(58) Volkman, J. K. A review of sterol markers for marine and terrigenous organic matter. *Org. Geochem.* **1986**, *9*, 83−99.
(59) Tissot, B. P.; Welte, D. H. *Petroleum Formation and Occurrence*; Springer-Verlag: New York, 1984.
(60) Rangel, A.; Osorno, J. F.; Ramirez, J. C.; De Bedout, J.; González, J. L.; Pabón, J. M. Geochemical assessment of the Colombian oils based on bulk petroleum properties and biomarker parameters. *Mar. Pet. Geol.* **2017**, *86*, 1291−1309.
(61) Rimmer, S. M. Geochemical paleoredox indicators in Devonian−Mississippian black shales, Central Appalachian Basin (USA). *Chem. Geol.* **2004**, *206*, 373−391.
(62) Wei, Z. F.; Wang, Y. L.; Wang, G.; Sun, Z. P.; Zhang, T.; Xu, L.; Ma, X. Y.; He, W. Paleoenvironmental conditions of organic-rich Upper Permian Dalong Formation shale in the Sichuan Basin, southwestern China. *Mar. Pet. Geol.* **2018**, *91*, 152−162.
(63) Welte, D. H.; Ebhardt, G. Distribution of long chain n-paraffins and n-fatty acids in sediments from the Persian Gulf. *Geochem. Cosmochim. Acta* **1968**, *32*, 465−466.
(64) Welte, D. H.; Waples, D. W. Über die Bevorzugung geradzahliger n-alkane in Sedimentgesteinen. *Die Naturwissenschaften* **1973**, *60*, 516−517.
(65) Wignall, P. B.; Newton, R. Pyrite framboid diameter as a measure of oxygen deficiency in ancient mudrocks. *Am. J. Sci.* **1998**, *298*, 537−552.
(66) Wilkin, R. T.; Arthur, M. A.; Dean, W. E. History of water-column anoxia in the Black Sea indicated by pyrite framboid size distributions. *Earth Planet Sci. Lett.* **1997**, *148*, 517−525.
(67) Yan, D. T.; Wang, H.; Fu, Q. L.; Chen, Z. H.; He, J.; Gao, Z. Geochemical characteristics in the Longmaxi Formation (Early Silurian) of South China: Implications for organic matter accumulation. *Mar. Pet. Geol.* **2015**, *65*, 290−301.
(68) Wei, H. Y.; Wei, X. M.; Qiu, Z.; Song, H. Y.; Shi, G. Redox conditions across the G-L boundary in South China: Evidence from pyrite morphology and sulfur isotopic compositions. *Chem. Geol.* **2016**, *440*, 1−14.
(69) Wignall, P. B.; Newton, R.; Brookfield, M. E. Pyrite framboid evidence for oxygen-poor deposition during the Permian-Triassic crisis in Kashmir. *Palaeogeogr. Palaeoclimatol. Palaeoecol.* **2005**, *216*, 183−188.
(70) Ibach, L. E. J. Relationship between sedimentation rate and total organic carbon content in ancient marine sediments. *AAPG Bull.* **1982**, *66*, 170−188.
(71) Wei, H. Y.; Chen, D. Z.; Wang, J. G.; Yu, H.; Tucker, M. E. Organic accumulation in the lower Chihsia Formation (Middle Permian) of South China: constraints from pyrite morphology and multiple geochemical proxies. *Palaeogeogr. Palaeoclimatol. Palaeoecol.* **2012**, *353*−*355*, 73−86.
(72) Wang, Z. W.; Fu, X. G.; Feng, X. L.; Song, C.; Wang, D.; Chen, W. B.; Zeng, S. Q. Geochemical features of the black shales from the Wuyu Basin, southern Tibet: Implications for palaeoenvironment and palaeoclimate. *Geol. J.* **2017**, *52*, 282−297.

https://doi.org/10.1021/acsomega.3c00273
ACS Omega 2023, 8, 16748−16761